Measurement of the response function of a custom plastic scintillator using monoenergetic neutron and proton sources

Aya Kanj, Clément Lynde, Frédérick Carrel, Mehdi Ben Mosbah, Julien Venara, Ziad El Bitar, Marc Rousseau, Richard Babut

Measurement of the response function of a custom plastic scintillator using monoenergetic neutron and proton sources

Aya Kanj, Clément Lynde, Frédérick Carrel, Mehdi Ben Mosbah, Julien Venara, Ziad El Bitar, Marc Rousseau, Richard Babut

***Abstract*— An experimental study was carried out to determine the light output function of the protons deposited energy in a custom triple discriminating (thermal neutrons/fast neutrons/gamma rays) plastic scintillator. Two response functions of the plastic scintillator were measured and compared using monoenergetic sources of either neutrons or protons. The response function to neutrons was measured at the IRSN Amande facility in CEA Cadarache using the monoenergetic neutron generator. The response matrix was based on six incident neutron energies that ranged from 953 keV to 14.8 MeV. The low energy threshold for detecting neutrons is evaluated at around 1 MeV. The second response function was measured utilizing the *Cyrcé* cyclotron at IPHC located in Strasbourg. The response matrix was obtained based on six incident proton energies ranging from 5.9 MeV to 19.97 MeV. The response function measured using monoenergetic neutrons has a nearly rectangular shape that extends from the light output of the low energy discrimination threshold to the light output of the full incident neutron energy. The pulse height spectra acquired with monoenergetic protons exhibit a Gaussian shape where the average value corresponds to the light output of the incident protons' energy. The exponential curve used to fit the light output data acquired from the monoenergetic neutron field generator aligns well with the light output data obtained from the monoenergetic proton beam.**

***Index Terms*—Plastic scintillator, proton light output, monoenergetic neutron source, monoenergetic proton beam.**

I. Introduction

PLASTIC scintillators are presently utilized as the primary components of numerous neutron measurement systems, enabling the determination of precise neutron energy spectra information and presenting a significant interest in fields such as nuclear material control, radiation protection, and homeland security fields [1]. Plastic scintillators provide many advantages over liquid scintillators, such as their low cost, non-toxic, and nonflammable properties. Moreover, due to their hydrogen-rich composition, plastic scintillators are ideal for fast neutron detection. Plastic scintillators possess isotropic response, resulting in unaltered neutron energy deposition, regardless of their direction. Furthermore, several studies suggest that doping plastic scintillators with lithium-6 [2,3] and boron [4] enhances their ability to detect thermal neutrons. Plastic scintillators detect ionizing radiation through emission of photons in the visible part of the light spectrum. The light emitted is typically non-linearly correlated with the energy deposited, owing to the quenching effect as per Birks' Law [2]. The primary light emission source occurs when neutrons interact with plastic scintillators through single or double elastic scattering on hydrogen. Carbon nuclei may also experience elastic scattering and other interactions, such as $^{12}C(n, \alpha)\,^{9}Be$ at the threshold of 6.19 MeV, $^{12}C(n, n3\alpha)$ at the threshold of 8.8 MeV, $^{12}C(n, p)^{12}Be$ at the threshold of 13.7 MeV and $^{12}C(n, d)^{11}Be$ at the threshold of 14 MeV [2]. In addition, in ^{6}Li-doped plastic scintillators, thermal neutrons are detected through the $^{6}Li(n,\alpha)^{3}H$ neutron capture reaction, which has a high cross section of 940 barns at a neutron energy of 0.025 eV [3]. However, for the same amount of recoil energy, alphas, and tritons create less light than protons, and the carbon recoil nuclei can only receive up to 28% of the kinetic energy from the incident neutron [2,4]. To accurately determine the neutron energy spectra, a fine calibration is required to establish the relation between the incident neutron energy and the measured light output. To this aim, it is common to measure the response function with a monoenergetic neutron source. In most cases, the response function of plastic scintillators to fast neutrons is dominated by the energy deposited by the recoil protons from the elastic collision of neutrons with hydrogen. Hence, we suggest an alternative approach for measuring the light output of protons by directly using a monoenergetic proton source.

In this work, two calibration methods using monoenergetic neutron field generator and a monoenergetic proton beam were compared to measure the proton light output of a custom triple discriminating plastic scintillator.

II. Method

A. Experimental set-up

In the frame of our study, we considered a custom plastic scintillator with triple discrimination capabilities (gamma rays/fast neutrons/thermal neutrons). This scintillator, manufactured by CEA List, is composed of 73.15% of styrene

Aya Kanj and Frédérick Carrel are with Université Paris-Saclay, CEA, List, F-91120, Palaiseau, France (e-mail: aya.kanj@cea.fr).

Clément Lynde was with Université Paris-Saclay, CEA, List, F-91120, Palaiseau, France. He is now with Université Paris Saclay, CEA, Service de physico-chimie, 91191 Gif-sur-Yvette Cedex, France.

Mehdi Ben Mosbah is with Laboratoire de mesure nucléaire (LMN), CEA-Cadarache, F-13108 St-Paul-lez-Durance, France.

Julien Venara is with Laboratoire d'étude des technologies numériques et des procédés avancés (LNPA), CEA-Marcoule, F-30207 Bagnols-sur-Cèze, France.

Ziad El Bitar and Marc Rousseau are with Institut Pluridisciplinaire Hubert Curien, IN2P3, CNRS, 67200 Strasbourg, France.

Richard Babut is with IRSN Cadarache, SDOS/LMDN, F-13108 Saint-Paul-lez-Durance, France.

monomer, 8.13% of methacrylic acid, 16.26% of PPO primary fluorophore, 0.024% of 1.4-bis(5-phenyloxazol-2-yl) benzene (POPOP) and 2.44% of Liα-valerate (Liαval). The light yield of the scintillator is 7920 ph/MeV. A detailed description can be found in reference [5] for further information on the plastic scintillator.

The experimental set-up, shown in Fig. 1, consists of a 1×1×2 cm^3 rectangular plastic scintillator coupled to a (2×2) Silicon Photomultiplier (SiPM) from Onsemi [6]. Each pixel of the SiPM measures 6.5×6.5 mm^2, and the overall size of the SiPM is 13×13 mm^2. The plastic scintillator and SiPM are both enclosed with a 0.1 mm layer of polytetrafluoroethylene (PTFE) and a 0.07 mm layer of aluminum. The SiPM is connected to the scintillator's edge, which measures (1×1 cm^2). We use the CAEN digitizer DT5743 to convert the input signal into digital data [7]. For the power supply, we use a CAEN high-voltage regulator DT5485 [8]. The discrimination between thermal neutrons, fast neutrons, and gamma rays is performed by using the optimized PSD (Pulse Shape Discrimination) method described in [9].

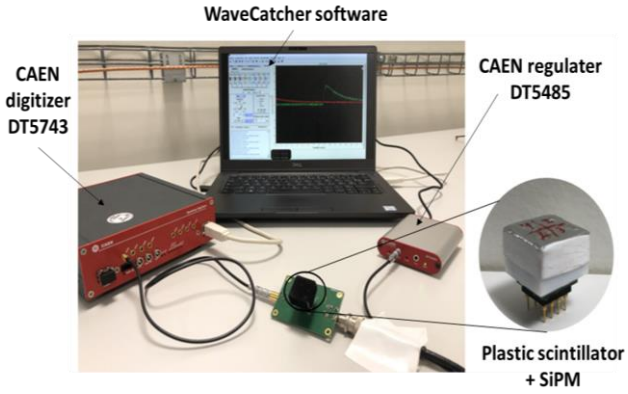

Fig. 1 Main building blocks of the experimental set-up

B. *Gamma calibration*

Gamma calibration is applied to convert the measured parameter total charge *Q*, the area of the pulse acquired by the digitizer, into deposited energy by gamma rays expressed in MeVee (MeV electron equivalent) or light equivalent. The measured pulse height spectrum was calibrated using gamma sources of ^{22}Na (0.511 MeV, 1.274 MeV), ^{137}Cs (0.661 MeV), and ^{241}Am (0.059 MeV).

For gamma energies above 0.1 MeV, the Compton scattering effect is the dominant reaction against photo-electric absorption due to the low *Z* of the material. Therefore, the Compton edges of the gamma rays spectra are used for calibration with ^{22}Na and ^{137}Cs, and the full-energy peak of the gamma rays spectrum is used for calibration with ^{241}Am.

To perform the gamma calibration, we have applied the iterative method described in reference [10]. In this method, the simulated spectra from the MCNP6.2 Monte Carlo code [11] are fitted to match the measured spectra for the determination of the Compton maximum values and the detector's energy resolution. To calculate the detector's energy resolution, a new GEB (Gaussian Energy Broadening) set of parameters is derived from the experimental spectra and applied to the simulation at each iteration. In order to determine the GEB parameters (a, b, c), the energy broadening effect in the measured spectra is calculated by determining the Full Width at Half Maximum (FWHM) of Gaussian distributions that fit the measured spectra at positions of Compton maximum or full-energy-peak. The calculation is conducted in accordance with equation (1), where E refers to the initial deposited energy before broadening.

$$FWHM = a + b\sqrt{E + cE^2} \tag{1}$$

After two iterations, Fig. 2 illustrates the calibration curve presented by a quadratic equation and the GEB parameters finally obtained. In addition, Fig. 3 displays a good agreement between the simulated and measured spectra for the ^{22}Na source (R^2=0.966) and for the ^{137}Cs source (R^2=0.962). However, there is less accordance in the simulated and measured spectra of the ^{241}Am source (R^2=0.899). This difference can be explained by the ^{241}Am full absorption peak (59.5 keV) being close to the low-energy threshold for gamma-ray detection.

The results indicate that this iterative method effectively calibrates detector energy and brings the simulation closer to reality.

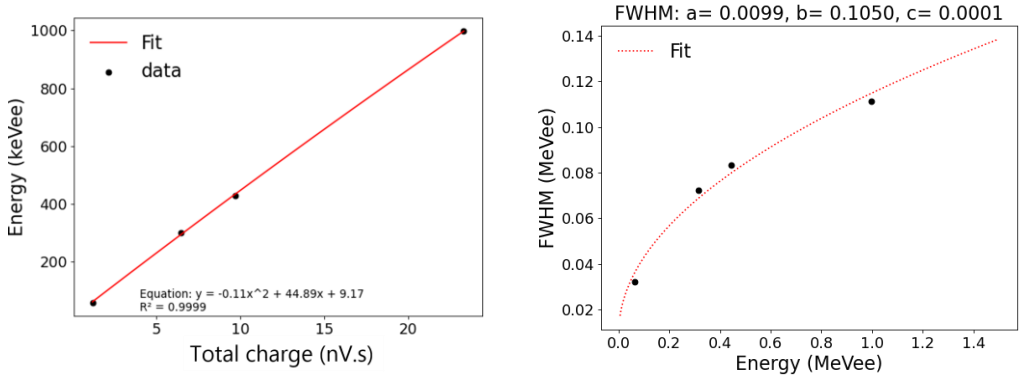

Fig. 2 At left: energy calibration curve of the custom plastic scintillator using ^{22}Na, ^{137}Cs, and ^{241}Am gamma sources. At right: full width at half-maximum (FWHM) according to the gamma-ray energy for the custom plastic scintillator.

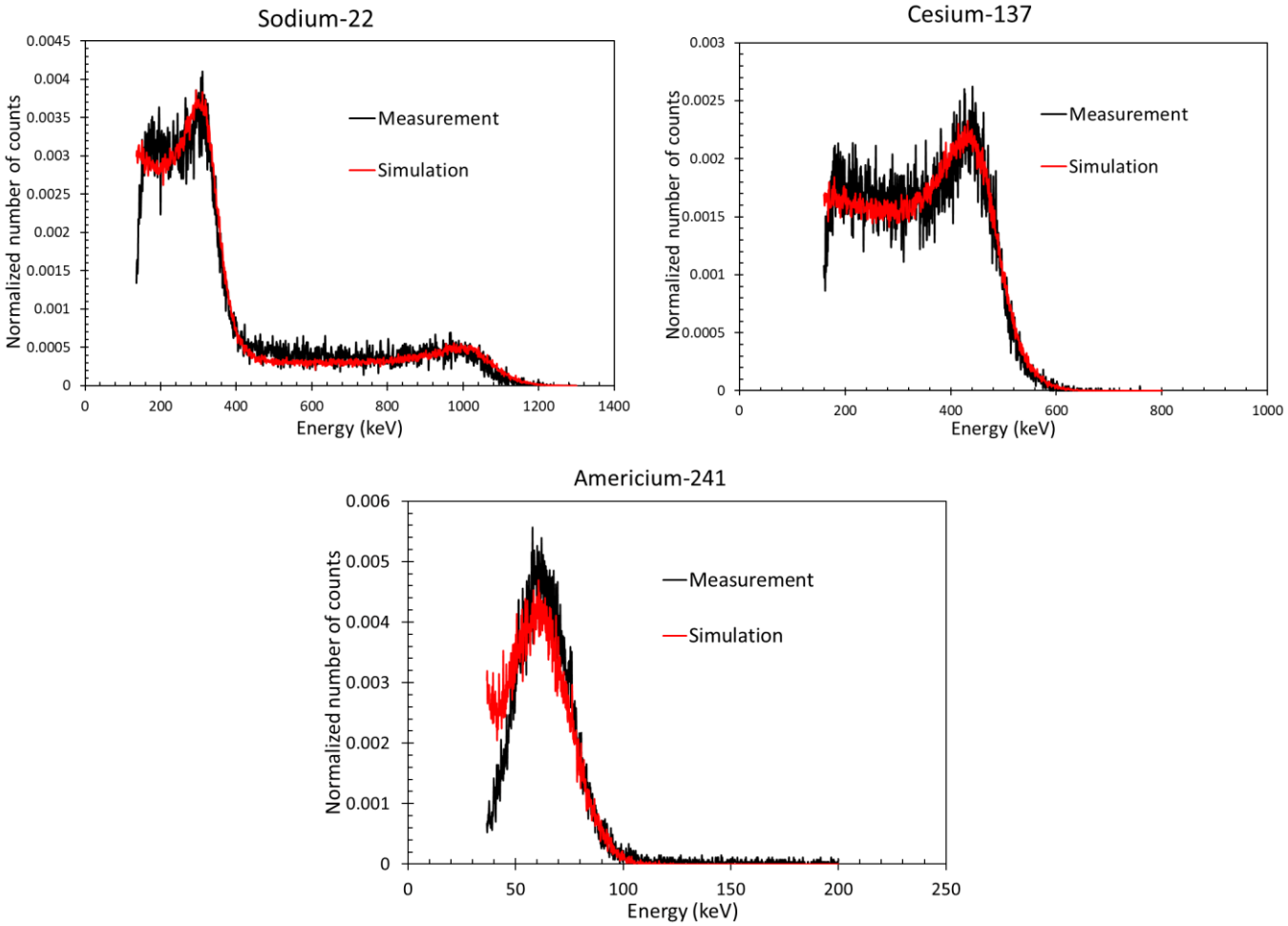

Fig. 3 Comparison between measured and simulated pulse height spectra of ^{22}Na, ^{137}Cs, and ^{241}Am.

III. Experimental Results

A. Measurement of the response matrix by using the monoenergetic neutron fields

The Amande facility [12] is based on an ion accelerator delivering protons or deutons in the range from 100 keV to 4 MeV. The accelerated charged particles (protons or deutons) interact with a thin target (scandium, lithium, tritium, or deuterium) to produce monoenergetic neutron fields within a broad energy range of 2 keV to 20 MeV. To measure the response function of the custom triple discriminating plastic scintillator, we irradiate the scintillator with neutron fields of energy 191 keV, 320 keV, 400 keV, 480 keV, 953 keV, 1063 keV, 2062 keV, 4404 keV, 13400 keV, and 14800 keV. The Amande beam also emits gamma rays, which are created at the same time as neutrons when the proton beam interacts with the target. The discrimination between thermal neutrons, fast neutrons, and gamma rays is performed by using the optimized PSD (Pulse Shape Discrimination) method described in [9]. The histograms shown in Fig. 4 correspond to data obtained with the triple-discriminant plastic scintillator ($n_{rapid}/n_{thermal}/\gamma$) doped with ^{6}Li. For neutron energies between 191 and 953 keV, we find the gamma component (bottom) and a second component (top). The latter, for all energies between 191 and 953 keV, is found in the same channel, whose total charge value is estimated at around 8 nV.s. This feature shows that this component is due to thermal neutron capture by ^{6}Li via the ^{6}Li(n, α)^{3}H reaction. In the histograms shown in Fig. 5, for incident neutron energies between 2062 keV and 14800 keV, we find the gamma component (bottom) and the fast neutron component (top). For the 1063 keV neutron histogram, all three components exist at the same time, we find the gamma component at the bottom, the fast (first cloud) and thermal (second cloud) neutrons components at the top. This result shows that the low-energy threshold for fast neutrons detected by interaction with protons is around 1063 keV.

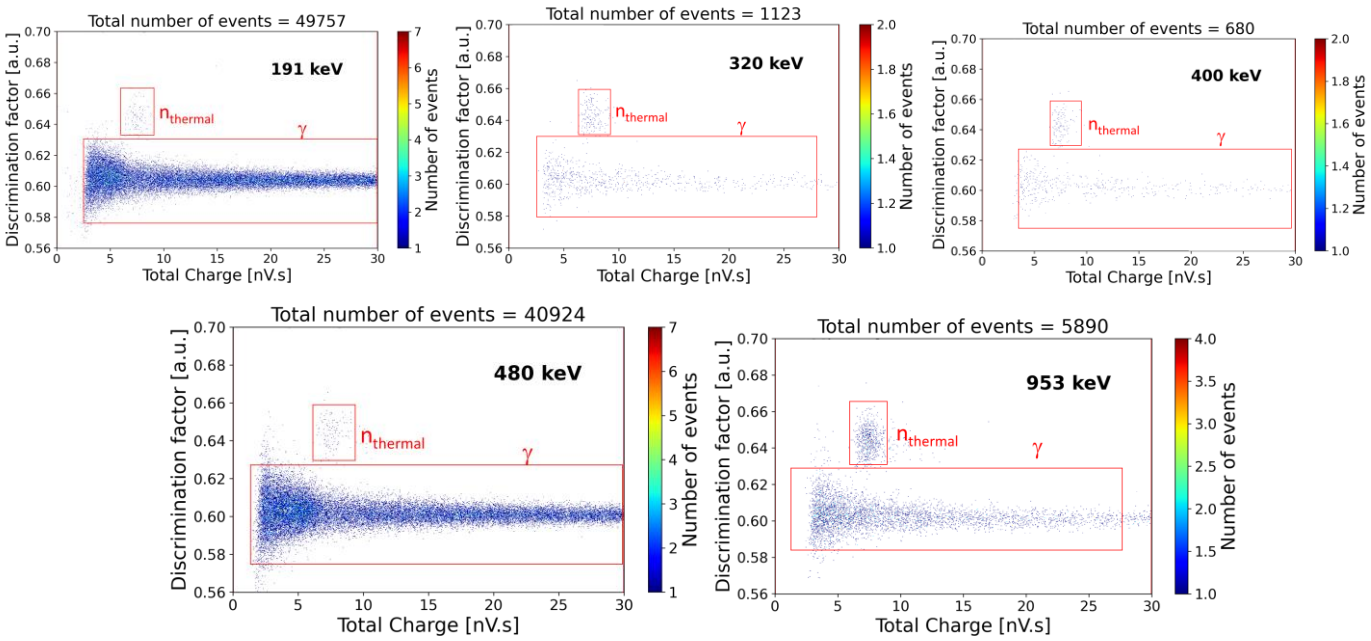

Fig. 4 Two-dimensional histograms showing the distribution of the number of events as a function of energy and discrimination factor (Qtail/Qtot) for the incident neutron of energy 191 keV, 320 keV, 400 keV, 480 keV, and 953 keV. The acquisition times for these measurements are 9 min, 15 min, 5 min, 9 min, and 37 min respectively.

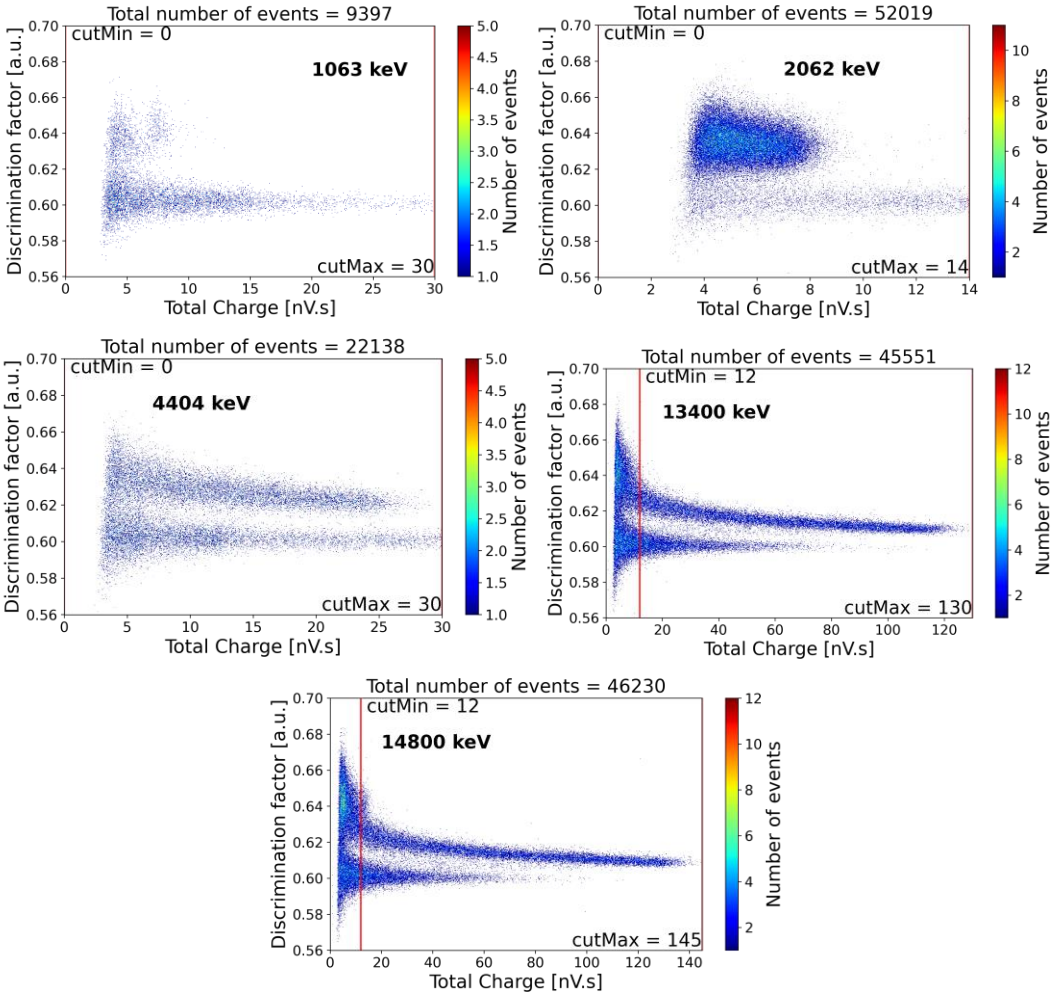

Fig. 5 Two-dimensional histograms showing the distribution of the number of events as a function of energy and discrimination factor (Qtail/Qtot) for the incident neutron of energy 1063 keV, 2062 keV, 4404 keV, 13400 keV, and 14800 keV. The acquisition times for these measurements are 26 min, 15 min, 6 min, 5 min, and 3 min respectively.

The response matrix is constructed using data from six incident neutron energies ranging from 1063 keV to 14800 keV. Fig. 6 shows scintillator responses, measured in keVee, for neutrons with energies of 1063 keV, 2062 keV, 4404 keV, 13400 keV, and 14800 keV.

In the ideal case, a recoil proton light output spectrum is described by a uniform distribution with the maximum energy edge equal to the energy of the incident neutrons. In practice, the full-energy deposition edge is smeared due to the effects of detector resolution and multiple scatters near the edge location. In this work, we determined the position of the full-energy deposition edge by determining the highest energy minimum of the first derivative of the light output spectrum edge. This method is described in [13]. The light output spectrum is smoothed, and a Gaussian distribution is used to fit the highest-energy minimum of the first derivative near the spectrum's edge. The centroid of the Gaussian represents the position of the full-energy deposition edge, and the standard deviation of the gaussian is used for estimating the error associated with each data point. In the plot of the 1063 keV neutron energy spectrum of Fig. 6, the dip at low energy correspond to fast neutrons while the dip at high energy correspond to thermal neutrons. However, the peak around 220 keVee may be influenced by the high threshold level in the spectrum measurement. To account for this, an additional error equivalent to 20% of the value was incorporated into the error estimation.

The resulting calibration curve, which relates the light output (in MeVee) to the recoil proton energy deposition expressed in MeVep (MeV equivalent proton), is shown in Fig. 7.

The exponential function (2) was utilized to fit data according to the empirical law specified in reference [14].

$$L = aE_p - b(1 - \mathrm{e}^{-cE_p}) \tag{2}$$

Where L is the light response expressed in MeVee, E_p is the recoil proton energy expressed in MeVep, and a, b, and c are the free parameters to be adjusted. These parameters are calculated to have the following values: $a = 0.58$, $b = 2.55$ and $c = 0.19$. Fig. 7 illustrates a comparison made between the proton light output of the custom triple discriminating plastic scintillator (2 cm³) and the EJ276 from [2], a commercial

double discriminating plastic scintillator (12.87 cm³). Given that it has been shown that the proton light output remains unaffected by both the size of the scintillator [15] and its chemical composition [16], the variance in proton light output can be attributed to the impact of the non-linear response of the SiPM. However until now we have not developed a method to rule out the influence of the SiPM. This aspect will be addressed in future investigations [17].

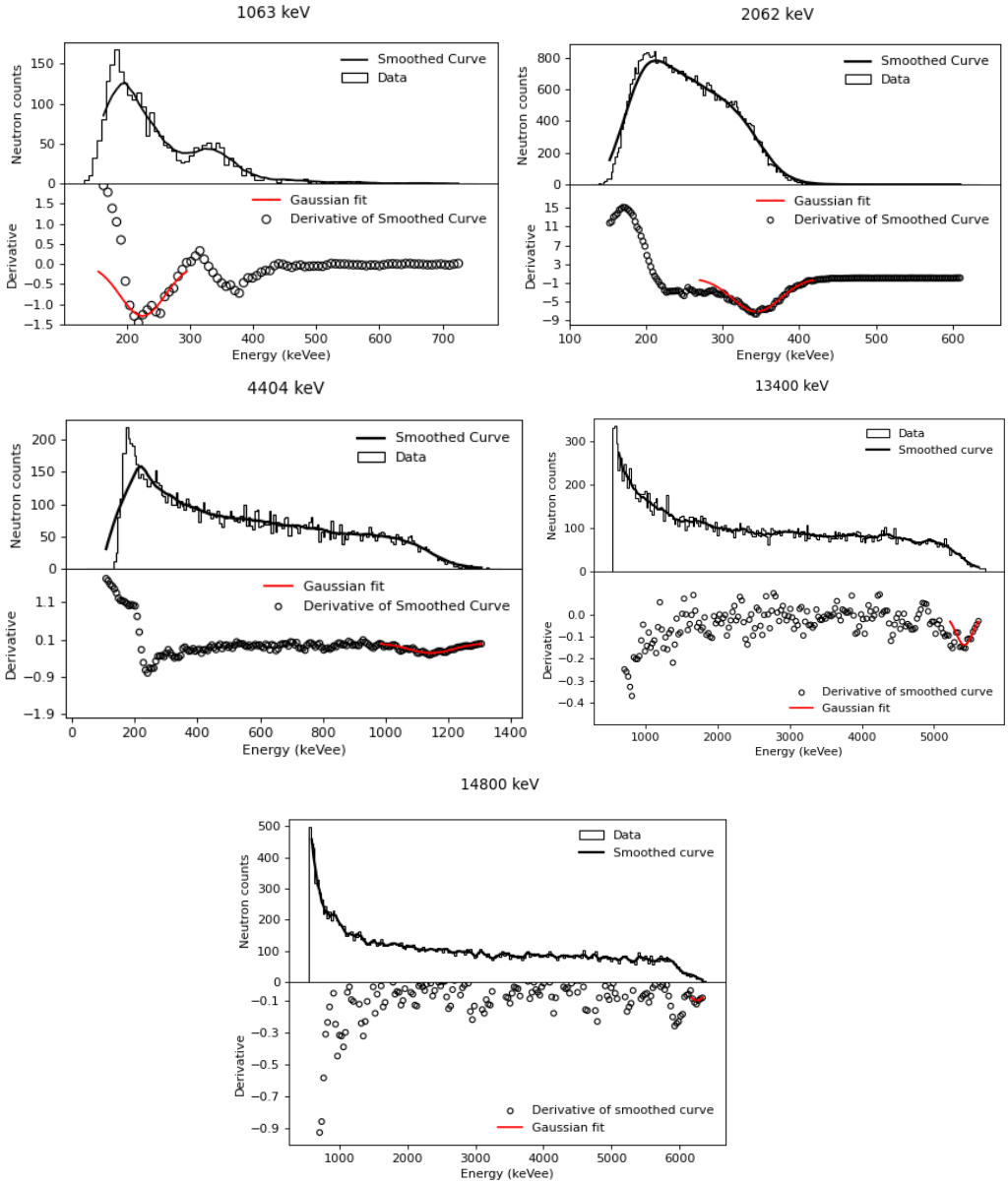

Fig. 6 Measured neutron response function of the custom triple-discriminant plastic scintillator according to the incident neutron energy.

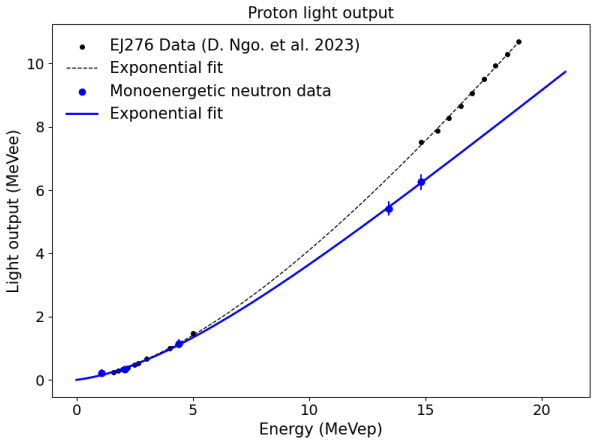

Fig. 7 Light output as a function of energy deposited by recoil protons in the 2 cm^3 triple-discriminant scintillator using data extracted from the calibration performed with the neutron source (blue line), compared with the results reported in [2] for an EJ276 cylindrical scintillator with a diameter of 2.54 cm and a height of 2.54 cm (black line).

B. Measurement of the response matrix by using a monoenergetic proton beam

A second response function was measured at the *Cyrcé* facility in front of the TR24 cyclotron that produces protons with energies ranging from 16 MeV to 25 MeV and up to 500 µA in Strasbourg's Institut Pluridiciplnaire Hubert Curien (IPHC/CNRS) [18]. To adjust the proton beam's initial energy, aluminum screens of different thicknesses were employed. The *Cyrcé* facility provides an automated beam collimation system. This allowed for precise control over the direction and width of the emitted beam. The scintillator was placed in front of a 3 mm collimator, through which protons were emitted. The scintillator was exposed to nine different proton energies: 0.81 MeV, 3 MeV, 3.92 MeV, 5.97 MeV, 7.24 MeV, 10 MeV, 13.7 MeV, 14.33 MeV, and 19.97 MeV. Fig. 8 displays the energy spectra of the recoil protons at each energy.

Only protons with energies above 5.97 MeV are detected among the emitted proton energies. However, we are aware that the low energy detection threshold for neutrons (and hence for protons) is approximately 1 MeV. The fact that protons with energies below 5.97 MeV are not detected at *Cyrcé* is due to the presence of PTFE and aluminum layers encasing the scintillator. Protons interact with these surrounding layers, depositing some of their energy before reaching the scintillator. This phenomenon decreases the energy of the incident protons. For protons with energy below 5.97 MeV, their energy drops below the low energy detection threshold. For protons with energies above 5.97 MeV, this phenomenon directly impacts their energy upon reaching the scintillator. For this reason, to precisely produce the calibration curve correlating the proton energy deposition (expressed in MeVep) and the light response (expressed in MeVee), it is necessary to investigate the effect of these materials on the proton beam's energy.

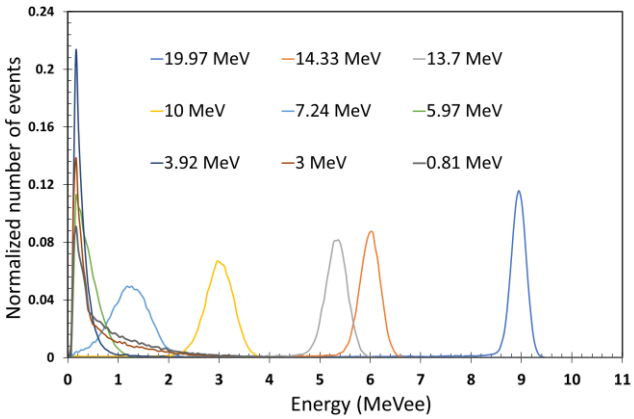

Fig. 8 Triple discriminant scintillator proton response function measured using the monoenergetic proton beam. Each response is associated with the energy of the protons emitted by the beam, not those deposited in the scintillator.

We performed a Monte Carlo simulation utilizing the MCNP6.2 code of a proton beam interacting with a triple discriminating plastic scintillator, measuring 2 cm^3, covered by PTFE and aluminum layers. To study the impact of PTFE and aluminum on the energy of protons hitting the scintillator, we ran a batch of simulations while varying the thickness of these materials. In addition, we varied the scintillator-to-beam distance to investigate the impact of air on proton energy. Fig. 9 displays graphs illustrating the proton energy deposition based on their incident energy and the materials traversed. Aluminum has the most significant impact on the energy deposited by protons, considering its density. Furthermore, we observed that slight variations in the thickness of the three materials, specifically 0.1 mm for PTFE and aluminum and 0.5 cm for air, significantly impact the amount of energy deposited by protons. Our experimental configuration consists of 10 mm of air, 0.1 mm of PTFE, and 0.07 mm of aluminum separating the scintillator and the proton beam. Taking into account the influence of these three materials, Table I presents the energy of protons that reach the scintillator after passing through the mentioned materials, starting with air, followed by PTFE, and finally aluminum.

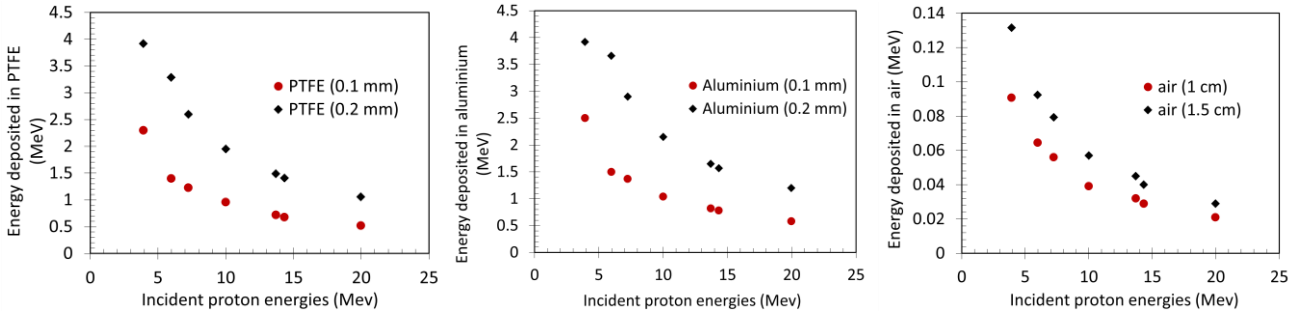

Fig. 9 Deposited energy as a function of the incident proton energy in the various materials (aluminum, PTFE, and air) surrounding the scintillator.

TABLE I SHOWS THE ENERGY OF PROTONS REACHING THE SCINTILLATOR AS A FUNCTION OF THE ENERGY OF PROTONS EMITTED BY THE BEAM AFTER INTERACTING WITH THE FOLLOWING THREE MATERIALS: AIR, PTFE, AND ALUMINUM.

Energy of the protons emitted by the beam (MeV)	Energy of the protons reaching the scintillator (MeV)
3	0
3.92	1.61
5.97	4.49
7.24	6.02
10	9.05
13.70	12.97
14.83	14.12
19.97	19.42

C. *Comparison of the two light response functions*

Considering proton energy deposited in the scintillator, shown in Table I, and their corresponding light equivalent energies, shown in Fig. 8, additional calibration points have been determined using the proton beam. These calibration points are then added to the calibration curve obtained using the neutron source, as shown in Fig. 10. The exponential curve that was fitted from the monoenergetic neutron generator accurately represents the light output data obtained from the monoenergetic proton beam.

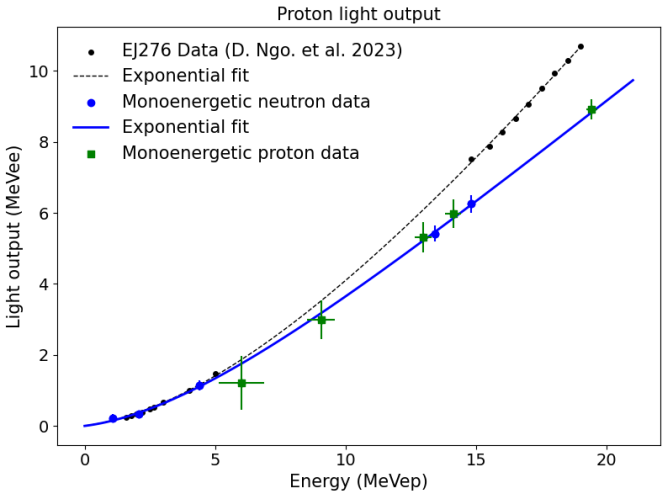

Fig. 10 Proton light output of the triple discriminating plastic scintillator obtained from neutron source (blue dots) and proton beam source (green dots), compared with the proton light output obtained in another work for EJ276 plastic scintillator (black dots) [2].

IV. DISCUSSION

The calibration points acquired through the use of the monoenergetic proton beam match well with the calibration curve derived from measuring data with the monoenergetic neutron generator. These results confirm the feasibility and potential of using a proton beam to directly assess the proton light response in the plastic scintillator.

This method offers several advantages, which are complementary to a monoenergetic neutron-based calibration step, and are as follows:

- The Gaussian shape of the light response facilitates the determination of calibration points;
- The absence of parasitic events such as gamma rays allows for more accurate measurements of proton light output and removes the need to discriminate between protons and gamma rays;
- The use of a proton beam, unlike a neutron generator, provides an extensive amount of calibration data for energies ranging from 5 MeV to 13 MeV;
- Automatic beam collimation constitutes an essential feature in achieving a pixel-by-pixel calibration of a pixelated plastic scintillator.

V. CONCLUSIONS AND FUTURE DEVELOPMENTS

In the present work, we utilized monoenergetic neutron and proton sources to determine the light output function for a custom triple discriminating plastic scintillator. We then compared the light output function of our sample with that of EJ276, a commercially available scintillator.

The use of the monoenergetic proton beam method serves as a complementary approach compared to a calibration step based on a monoenergetic neutron generator for carrying out a plastic scintillator energy calibration. However, a thorough understanding of the thickness of materials that the protons traversed before interacting with the scintillator is critical to calibrate the scintillator using a proton beam.

In upcoming investigations, we intend to perform pixel-by-pixel calibration of a plastic scintillator that is pixelated by 12×12 pixels, each measuring 3.6×3.6×3.6 mm^3, using the monoenergetic proton collimated beam. We will employ this pixelated scintillator in applications related to neutron imaging.

REFERENCES

[1] G. Corre, K. Boudergui, G. Sannie, V. Kondrasovs, Neutron Detection with Large Plastic Scintillators for RPM Applications, in: ANIMMA, Lisbon, Portugal, 2015: pp. 1–4. https://doi.org/10.1109/ANIMMA.2015.7465625.

[2] K.D. Ngo, C. Cazzaniga, M. Paoletti, D. Rigamonti, M. Kastriotou, C. Frost, M. Tardocchi, J. Sykora, S. Mann, B. Lutz, R. Nolte, Fast neutron response characterization of an EJ-276 plastic scintillator for use as a neutron monitor, Nucl Instrum Methods Phys Res A 1051 (2023). https://doi.org/10.1016/j.nima.2023.168216.

[3] G.F. Knoll, Radiation detection and measurement, 3rd ed., John Wiley & Sons, Inc., 2000. https://phyusdb.files.wordpress.com/2013/03/radiation detectionandmeasurementbyknoll.pdf.

[4] V. V. Verbinskit, W.R. Burrus +, T.A. Love, W. Zobel, N.W. Hill, R. Textor, Calibration of an organic scintillator for neutron spectrometry, Nuclear Instruments and Methods 65 (1968) 8–25. https://doi.org/10.1016/0029-554X(68)90003-7.

[5] C. Frangville, M. Hamel, G. Bertrand, E. Montbarbon, C. Lynde, A. Grabowski, Large solubility of Lithium carboxylates reaching high rates of 6Li incorporation in polystyrene-based plastic scintillators for fast/thermal neutrons and gamma rays detection,

Mater Chem Front 3 (2019). https://doi.org/10.1039/C9QM00153K.

[6] ARRAYC-SERIES , Silicon Photomultipliers (SiPM) 4-Side Scalable Arrays, Datasheet, United States, 2023. www.onsemi.com.

[7] DT5743, CAEN Tools for Discovery (2023). https://www.caen.it/products/dt5743/ (accessed July 27, 2023).

[8] DT5485P, CAEN Tools for Discovery (2023). https://www.caen.it/products/dt5485p/ (accessed August 11, 2023).

[9] C. Lynde, E. Montbarbon, M. Hamel, A. Grabowski, C. Frangville, G.H. V Bertrand, G. Galli, F. Carrel, V. Schoepff, Z. El Bitar, Optimization of the Charge Comparison Method for Multiradiation Field Using Vari-ous Measurement Systems, IEEE Trans Nucl Sci 69 (2020) 679–687. https://doi.org/10.1109/TNS.2020.2966886ï.

[10] X. Li, Y. Wang, R. Zhou, C. Yan, Energy calibration for plastic scintillation detectors based on Compton scatterings of gamma rays, Journal of Instrumentation 12 (2017). https://doi.org/10.1088/1748-0221/12/12/P12025.

[11] J. Armstrong, F. B. Brown, J. S. Bull, L. Caswell, L. J. Cox, D. Dixon, R.A. Forster, J. T. Goorley, H.G. Hughes, J. Favorite, R. Martz, S.G. Mashnik, M.E. Rising, MCNP User's Manual Code Version 6.2., Los Alamos National Laboratory Tech. Rep. LA-UR-17-29981 (2017).

[12] V. Gressier, J.F. Guerre-Chaley, V. Lacoste, L. Lebreton, G. Pelcot, J.L. Pochat, T. Bolognese-Milstajn, D. Champion, AMANDE: A new facility for monoenergetic neutron fields production between 2 keV and 20 MeV, Radiat Prot Dosimetry 110 (2004) 49–52. https://doi.org/10.1093/rpd/nch185.

[13] N. V. Kornilov, I. Fabry, S. Oberstedt, F.J. Hambsch, Total characterization of neutron detectors with a 252Cf source and a new light output determination, Nucl Instrum Methods Phys Res A 599 (2009) 226–233. https://doi.org/10.1016/j.nima.2008.10.032.

[14] R. Katz, S.C. Sharma, M. Homayoonfar, Detection of energetic heavy ions*, Nuclear Instruments and Methods 100 100 (1971) 13–32.

[15] Sara Alawabdeh, Characterization and Comparison of Proton Light Yield of Similar Composition Organic Scintillators With Different Sizes, 2023.

[16] T.A. Laplace, B.L. Goldblum, J.E. Bevins, D.L. Bleuel, E. Bourret, J.A. Brown, E.J. Callaghan, J.S. Carlson, P.L. Feng, G. Gabella, K.P. Harrig, J.J. Manfredi, C. Moore, F. Moretti, M. Shinner, A. Sweet, Z.W. Sweger, Comparative scintillation performance of EJ-309, EJ-276, and a novel organic glass, Journal of Instrumentation 15 (2020). https://doi.org/10.1088/1748-0221/15/11/P11020.

[17] L. Brinkmann, E. Garutti, S. Martens, J. Schwandt, Correcting the Non-Linear Response of Silicon Photomultipliers, Sensors 24 (2024). https://doi.org/10.3390/s24051671.

[18] Platforme CYRCé, IPHC Institut Pluridisciplinaire Hubert Curien Strasbourg (2023). https://cyrce.fr/.